ACSNANO

www.acsnano.org

ARTICLE

Unravelling the Mechanism of Viscoelasticity in Polymers with Phase-Separated Dynamic Bonds

Sirui Ge, Subarna Samanta,* Bingrui Li, G. Peyton Carden, Peng-Fei Cao, and Alexei P. Sokolov*

Cite This: https://doi.org/10.1021/acsnano.2c00046 Read Online

ACCESS | Metrics & More | Article Recommendations | Supporting Information

ABSTRACT: Incorporation of dynamic (reversible) bonds within polymer structure enables properties such as self-healing, shape transformation, and recyclability. These dynamic bonds, sometimes refer as stickers, can form clusters by phase-segregation from the polymer matrix. These systems can exhibit interesting viscoelastic properties with an unusually high and extremely long rubbery plateau. Understanding how viscoelastic properties of these materials are controlled by the hierarchical structure is crucial for engineering of recyclable materials for various future applications. Here we studied such systems made from short telechelic polydimethylsiloxane chains by employing a broad range of experimental techniques. We demonstrate that formation of a percolated network of interfacial layers surrounding clusters enhances mechanical modulus in these phase-separated systems, whereas single chain hopping between the clusters results in macroscopic flow. On the basis of the results, we formulated a general scenario describing viscoelastic properties of phase-separated dynamic polymers, which will foster development of recyclable materials with tunable rheological properties.

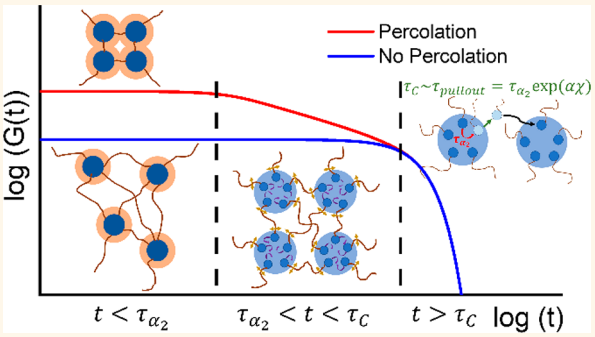

KEYWORDS: *associating polymers, network rearrangement, phase separation, interfacial layer, mechanical reinforcement, dynamic bonds*

INTRODUCTION

Polymers with dynamic bonds constitute an increasingly promising class of functional materials, where polymer chains are bonded together by reversible covalent[1−3] (e.g., vitrimers) or noncovalent (e.g., hydrogen and ionic bonds) interactions.[4−8] Because of the reversible nature of these transient interactions, it helps not only for developing functional materials such as self-healing ability and extreme stretchability,[9,10] shape memory,[11,12] and controlled stress relaxation but also makes them easy-to-process/recyclable.[13,14] The common interaction type is binary in nature, where two complementary groups form reversible bonds. The important parameter regarding this bond is the binding/dissociation energy along with the lifetime of the transient bonds,[15] which can be tuned based on the chemistry of the functional groups. At shorter time scale, material with these sticky bonds behaves as a network, whereas at time scale longer than that of the bond dissociation, the restriction to material flow is removed. However, this simple picture gets increasingly complicated in the presence of hierarchical structures within the material. Spider silk is one such example from the natural world, where H-bonds between adjacent β-strands of repetitive alanine/alanine-glycine moieties form nanocrystalline domains.[16] These β-sheet nanocrystals act as load-bearing cross-linking clusters within the glycine-rich amorphous matrix, endowing them with high elasticity and exceptional toughness/strength surpassing man-made fibers like Kevlar.[17]

Similar strategies have been employed in designing tough high-performance elastomers.[18−20] This type of nanophase separation can be achieved synthetically when the functional groups are immiscible with polymer matrix and phase-segregate in clusters, as observed in ionomers,[21] associating polymers,[22−24] and recently in vitrimers.[25] Clusters having higher glass transition or melting temperature compared to that of polymer matrix result in a prolonged rubbery plateau.[24] Moreover, recent studies[26] suggest that structural relaxation in these clusters controls viscosity and terminal relaxation of the polymers with phase separated associating groups. However, a

Received: January 3, 2022
Accepted: February 25, 2022

ACS Publications © XXXX American Chemical Society

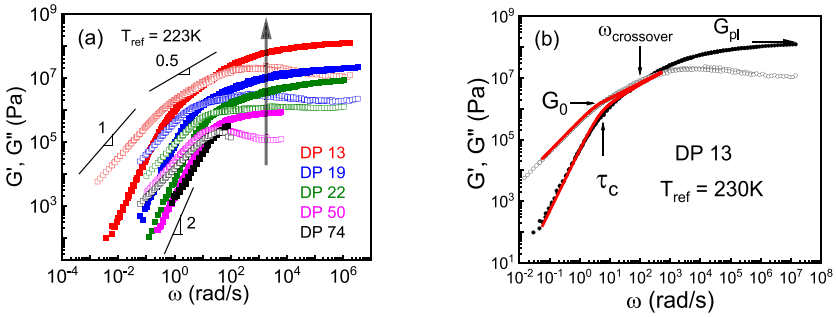

Figure 1. (a) Shear modulus master curves for the telechelic PDMS-COOH measured at temperatures higher than second T_g. The arrow indicates the increased rubbery plateau value for shorter chains. Slope of 0.5 indicates Rouse-like regime, whereas regime with $G' \approx \omega$ and $G'' \approx \omega^2$ at lower frequencies indicate terminal flow behavior of these polymers. (b) Master curve of the shear modulus for DP 13 sample based on the reference temperature of 230 K. Solid and open symbols refer to G' and G'' spectra, respectively. Fits based on the Rouse model are shown as red lines. τ_C refers to terminal relaxation of the material. The values of the rubbery plateau modulus (G_{Pl}) and shear modulus at terminal relaxation (G_0) are indicated with arrows. The crossover of G' and G'' is labeled as well, demonstrating that the estimation of the terminal relaxation time from the crossover is not accurate.

detailed microscopic understanding of how the network rearrangement occurs in the presence of phase separated clusters is still lacking. Simulations studies[27] suggested that structural rearrangements in this type of systems should go through fusion and dissociation of the clusters. This idea, however, was questioned in the recent experimental studies.[28,29] Moreover, a clear separation between the time scale of cluster's structural relaxation time and rheological terminal mode was observed and remains unexplained.[24,29]

Experiments[30−32] also indicated the presence of a thin interfacial polymer layer with restricted mobility around these clusters, which also results in the elevated rubbery plateau modulus explained by the mechanical interfacial layer model (ILM). However, the interfacial layers might overlap forming a percolated network.[33,34] Since the mechanical ILM assumes independent fillers with interfacial later,[35] the previous interpretation from mechanical ILM is questionable. For the polymer nanocomposites systems, the mechanical percolation model has already been utilized to describe the mechanical reinforcement in the presence of percolated network of the overlapping interfacial layers.[36−38] It has, however, never been used to study the analogous system like the phase separated associating polymers. Thus, the mechanism of network rearrangements and its effect on viscoelastic behavior in systems with clusters of the dynamic bonds remains a puzzle. Developing a microscopic understanding of viscoelasticity in polymers with clusters of dynamic bonds will help with rational design of materials with multifunctional properties and relatively easy recyclability.

To address this challenge, we provide a detailed analysis of the earlier studied model telechelic polymers with phase-separated functional end groups.[24,39] We demonstrate that the mechanical percolation model indeed explains well the unusually high rubbery plateau modulus in these materials. Most importantly, based on the analogy to block copolymers, we propose a mechanism of the network rearrangements via single chain hopping between clusters controlled by a thermodynamic energy barrier related to the immiscibility of the dynamic end groups and the polymer matrix. On the basis of these results, we propose a general scenario of viscoelasticity of polymers with clusters of dynamic bonds. The presented in-depth understanding provides design rules for developing functional materials with tunable viscoelastic properties.

RESULTS AND DISCUSSION

The telechelic PDMS-COOH used in this work consists of a backbone with polydimethylsiloxane (PDMS) terminated with 4-(propylamino)-4-oxobutanoic acid (COOH) (Figure S1). The telechelic PDMS-COOH has different degrees of polymerization (DP) of 13, 19, 22, 50, and 74.

Differential Scanning Calorimeters (DSC). Each of the investigated PDMS-COOH samples shows two glass transition steps in their heat flow spectra. The one at lower temperature (∼150 K) refers to the glass transition of the segmental motions of PDMS chains, while the one at higher temperature (∼200 K) originates from the end-group motions within the clusters (Figure S3).[24]

X-ray Scattering. Phase separation in PDMS-COOH has been verified through X-ray scattering in our previous publication.[32] The low-q weak result at around 0.1 Å $^{-1}$ indicates the phase separation. The similar X-ray scattering result was observed in DP 19 PDMS-COOH, which has not been studied before (Figure S4). The detailed analysis of X-ray scattering spectra[32] provides information on average center-to-center cluster distance (d) and radius of the cluster ($R_{cluster}$) (Table S1). The nearest cluster surface-to-surface distance can be calculated through $d_{IPS} = d - 2R_{cluster}$ (Table S1). With $R_{cluster}$, the grafting density (n_e) of PDMS chains on surface of the clusters can be calculated as

$$n_e = \frac{V_{cluster}}{S_{cluster} V_{end}} = \frac{R\rho N_A}{3M_{end}} \quad (1)$$

where M_{end} and ρ are the molecular weight and density of the associating chain end, respectively. N_A is the Avogadro's number. The grafting density was found to be ∼1.7−1.9 nm^{-2} for all associating polymers (Table S1).

Rheology. Small amplitude oscillatory shear was employed to measure linear viscoelastic behavior of the associating polymers. Shear modulus master curves were constructed (Figure 1a) by using time−temperature superposition (TTS) of the measured rheological spectra at different temperatures. The shift factor at various temperature used for TTS is shown in Figure S5. As was shown in our earlier studies,[32,39] the rubbery plateau modulus (G_{Pl}) increases as the chain length of the polymer backbone decreases, reaching an unusually high level of $G_{Pl} \approx 100$ MPa in the shortest chains with DP = 13 (Figure 1a).

https://doi.org/10.1021/acsnano.2c00046
ACS Nano XXXX, XXX, XXX−XXX

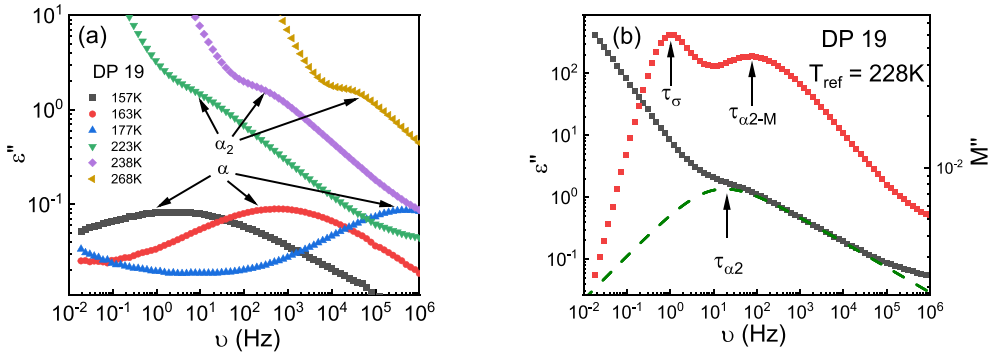

Figure 2. (a) Dielectric loss spectra for PDMS-COOH (DP 19) in the range of 10^{-2} to 10^{6} Hz. Loss peaks at low temperatures correspond to PDMS segmental motion (α-relaxation), while at higher temperatures, sticker motion within the cluster is visible as a separate process, termed as α_2 process. (b) Comparison of ε'' spectra and M'' spectra for telehelic PDMS-COOH with DP of 19 in which τ_{α_2}, τ_{α_2-M}, and τ_σ are labeled.

Terminal relaxation is observed at low frequencies where G' and G'' increase with frequency as ω^2 and ω^1, respectively. In addition, the samples with DP of 13, 19, and 22 exhibit an intermediate regime between the rubbery plateau and the terminal relaxation where both G' and G'' follow power law behavior $\sim\omega^{\alpha}$ with the exponent $\alpha \approx 0.5$ (Figure 1a). In contrast, this regime is absent in spectra of samples with DP 50 and DP 74, where the terminal relaxation is reached right after the end of the rubbery plateau (Figure 1a). In our previous publication, the terminal relaxation time was determined from the crossover of G' and G''.[24,39] However, this method is only valid for the Maxwellian relaxation behavior. Because of the presence of the Rouse-like spectra in lower DP samples, the crossover is no longer able to provide the accurate estimation of the terminal relaxation time (Figure 1b). In such case, the longest Rouse time scale is more accurate. Thus, to acquire the accurate terminal relaxation time (τ_C) as well as its corresponding shear modulus level (G_0), the Rouse model[40] is utilized to fit the shear modulus spectra:

$$G' = G_0 \sum_{j=1}^{N} \frac{\omega^2 {\tau_j}^2}{1 + \omega^2 {\tau_j}^2} \text{ and } G'' = G_0 \sum_{j=1}^{N} \frac{\omega \tau_j}{1 + \omega^2 {\tau_j}^2} \quad (2)$$

in which $\tau_j = \frac{\tau_c}{j^2}$. For PDMS-COOH with DP of 50 and 74, N is chosen to be 1, which corresponds to the Maxwell relaxation. However, for PDMS-COOH with DP of 13, 19, and 22, N is chosen to be an arbitrary number to fit the region of parallel decrease of the G' and G'' with slope of 0.5. The proposed fit describes well the shear modulus spectra (see, e.g., Figure 1b for PDMS-COOH with DP of 13) and provides estimates of both the G_{PI} and G_0 as well as τ_c.

Broadband Dielectric Spectroscopy (BDS). To analyze dynamics in the studied systems, we employed dielectric spectroscopy that revealed two major dielectric processes.[24,39] As a representative example, dielectric loss spectra (ε'') for the sample with DP 19 at several temperatures are shown in Figure 2a. Dielectric loss spectra for the rest of the samples are presented in Figure S6a–d. The process at lower temperatures is PDMS segmental motion (α-relaxation), while the process at higher temperatures is ascribed to motion of associating groups in the clusters, termed as α_2-relaxation.[24]

To compare rheological and dielectric data, the latter should be converted to the dielectric modulus M^* (ω):[41,42]

$$M^*(\omega) = \frac{1}{\varepsilon(\omega)} = M'(\omega) + iM''(\omega) \quad (3)$$

M'' spectra exhibit an additional dielectric process at lower frequencies (Figure 2b), which originate from conductivity relaxation (τ_σ).[43,44] We also noticed that the time scale of α_2 relaxation process from M'' (τ_{α_2-M}) is faster than that from ε'' spectra (τ_{α_2}). This is expected, as the relationship between characteristic relaxation time from M'' spectra (τ_M) and ε'' spectra (τ_ε) can be expressed by[45]

$$\tau_M = \frac{\varepsilon_{inf}}{\varepsilon_s}\tau_\varepsilon \quad (4)$$

in which ε_s and ε_{inf} indicate the dielectric constant in the limit of high and low frequencies. Thus, τ_{α_2-M} is shorter than τ_{α_2}, as was already emphasized in the literature.[15,32]

To acquire the characteristic relaxation time from modulus spectra, the M'' spectra were fit based on one Havrilliak-Negami (HN) function plus one Debye-like process for conductivity relaxation:

$$M''(\upsilon) = Im\left\{\frac{\Delta M_{\alpha_2}}{(1 + (2\pi\upsilon\tau_{HN-M})^{\beta_M})^{\gamma_M}} + \frac{\Delta M_\sigma}{1 + 2\pi i\upsilon\tau_\sigma}\right\} \quad (5)$$

in which ΔM_{α_2} and ΔM_σ are the "modulus strength" of α_2 process and conductivity process. τ_{HN-M} and τ_σ are the HN relaxation time for α_2 process and the conductivity relaxation time from dielectric modulus. β_M and γ_M are the stretching parameters for the α_2 process. The relaxation time corresponding to the peak position of α_2 process in M'' spectra is calculated using[46]

$$\tau_{\alpha_2-M} = \tau_{HN-M}\left[\sin\left(\frac{\beta_M\pi}{2 + 2\gamma_M}\right)\right]^{-1/\beta_M}\left[\sin\left(\frac{\beta_M\gamma_M\pi}{2 + 2\gamma_M}\right)\right]^{1/\beta_M} \quad (6)$$

Mechanical Percolation Model. Our previous studies revealed the existence of an interfacial polymer layer around the phase-separated clusters with a thickness $l_{int} \approx 0.8$–0.9 nm regardless of PDMS backbone length.[32] This small thickness was explained by the small radius of the phase separated clusters, $R_{cluster} \approx 1.4$–1.6 nm.[32] When the distance between clusters surfaces $d_{IPS} < 2l_{int}$, the interfacial layers overlap with

https://doi.org/10.1021/acsnano.2c00046
ACS Nano XXXX, XXX, XXX–XXX

each other, forming a percolating network. According to Table S1, the percolation of the interfacial regions can happen in PDMS-COOH with DP of 13, 19, and 22, while the interfacial layers are expected to be fairly separated in PDMS-COOH with DP of 50 and 74 (Figure 3). The critical volume fraction of the cluster, $(f_e)_c$, for percolation is estimated as $d_{IPS} \approx 2l_{int}$ and appears in the range ~13.5 ± 1.2 wt %.

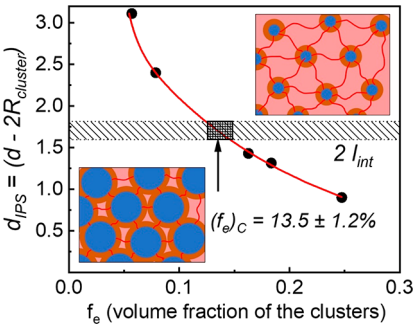

Figure 3. d_{IPS} as a function of f_e. Range of $2l_{int}$ value shown as a gray area. The box area indicates the estimated range of percolation threshold, $(f_e)_C$, when $d_{IPS} \approx 2l_{int}$. Above the percolation threshold, interfacial layers overlap to form a percolated network, whereas below the threshold, they are well separated. Blue circles represent the clusters of functional groups, which are surrounded by interfacial layers (orange) and linked by PDMS chains (red).

This analysis reveals that indeed interfacial layers form a percolating structure in systems with low DP, and the mechanical percolation model needs to be used to describe the elevated mechanical modulus observed in these samples. According to this model,[47] a composite modulus is expressed as

$$G_c = \frac{(1 - 2\psi + \psi X_r)G_s G_r + (1 - X_r)\psi G_r^{\,2}}{(1 - X_r)G_r + (X_r - \psi)G_s} \quad (7)$$

in which G_r is the shear modulus of the rigid phase. G_s is the shear modulus of the matrix (in this case PDMS matrix, which can be estimated from the classical rubber elasticity theory). X_r is the volume fraction of the overall rigid phase. ψ is the volume fraction of the spanning rigid phase formed in the percolated network through the overlapping of the interfacial layer and defined as

$$\psi = \begin{cases} 0, & X_r < X_c \\ X_r\left(\dfrac{X_r - X_c}{1 - X_c}\right)^b, & X_r \geq X_c \end{cases} \quad (8)$$

Here X_c is the volume fraction of the rigid phase at the percolation threshold; b is the percolation exponent characterizing the rate of the percolation structure formation with X_c.

We assume for simplicity that the clusters and their interfacial layers form a single rigid phase with volume fraction $X_r = \varphi_{cluster} + \varphi_{int}$. The mechanical percolation model (eqs 7 and 8) successfully describes the mechanical reinforcements in studied polymers (Figure 4). The value of X_r at the percolation threshold is found to be 56.5%, which corresponds to the critical volume fraction of the cluster, $(f_e)_c \approx 14.8\%$. The obtained value is in good agreement with the value estimated assuming an ordered cubic arrangement of the clusters (Figure 4). The critical exponent b obtained from the fit is ~1.7, which also agrees with the prediction from scalar elastic model in 3 dimensions developed by de Gennes.[48] Experimental investigations of percolation in various systems including organic polymer blends, polymer gels, and nanocomposite indicate the exponent b ranges from 1.6 to 2.2.[49−54] The model also provides the estimates of the shear modulus of the rigid phase, $G_r \approx 177$ MPa.

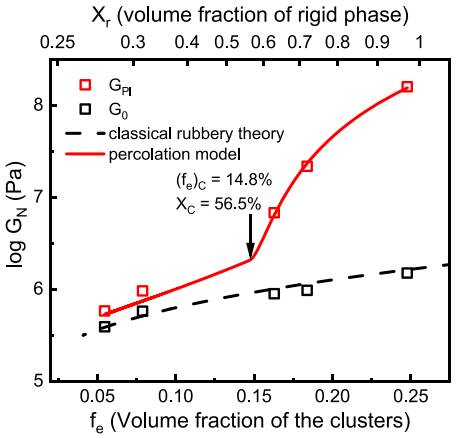

Figure 4. Variation of G_{PL} (red squares) and G_0 (black squares) as a function of f_e and X_r. Red line shows the fitting based on the mechanical percolation model (eqs 7 and 8). Black dashed line indicates the prediction from classical rubber elasticity theory. The arrow indicates the estimated from the fit percolation threshold.

The obtained G_r value agrees well with the estimates of the shear modulus of the rigid phase using the two-phase model (TPM) (Table 1). The two phases are clusters and the interfacial layer. The necessary parameters to estimate the shear modulus using TPM are shear modulus, volume fraction, and Poisson ratio of both clusters and the interfacial layer. The modulus of the interfacial layer was estimated to be ~100 MPa.[32] The Poisson's ratio of the interfacial layer (which consists of PDMS segments) is taken from literature[55] based on the PDMS values. For clusters, the modulus and the Poisson's ratio are assumed to be 3 GPa and 0.33, respectively, which are typical values for glassy hydrogen-bonded systems such as glycerol.[56] The volume fraction of cluster and interfacial layer in the rigid phase were estimated as $\varphi_{cluster,TPM} = \frac{\varphi_{cluster}}{\varphi_{cluster} + \varphi_{int}}$ and $\varphi_{int,TPM} = \frac{\varphi_{int}}{\varphi_{cluster} + \varphi_{int}}$, respectively, where values of $\varphi_{cluster}$ and φ_{int} for PDMS-COOH with DP of 13, 22, 50, and 74 were taken from previously published

Table 1. DP, Volume Fraction of Clusters $\varphi_{cluster}$, Volume Fraction of the Interfacial Layer φ_{int}, Volume Fraction of Clusters in Rigid Phase $\varphi_{cluster,TPM}$, Volume Fraction of Interfacial Regions in Rigid Phase $\varphi_{int,TPM}$, and Overall Shear Modulus of Rigid Phase Estimated Using TPM for PDMS-COOH Associating Polymers

material	DP	$\varphi_{cluster}$ (%)	φ_{int} (%)	$\varphi_{cluster,TPM}$ (%)	$\varphi_{int,TPM}$ (%)	G_r(TPM) (MPa)
PDMS-COOH	13	24.7	71.8	25.6	74.4	171
	19	18.4	59.1	23.7	76.3	164
	22	16.3	40.8	28.5	71.5	183
	50	7.9	26.6	22.9	77.1	161
	74	5.7	19.7	22.4	77.6	159

https://doi.org/10.1021/acsnano.2c00046
ACS Nano XXXX, XXX, XXX−XXX

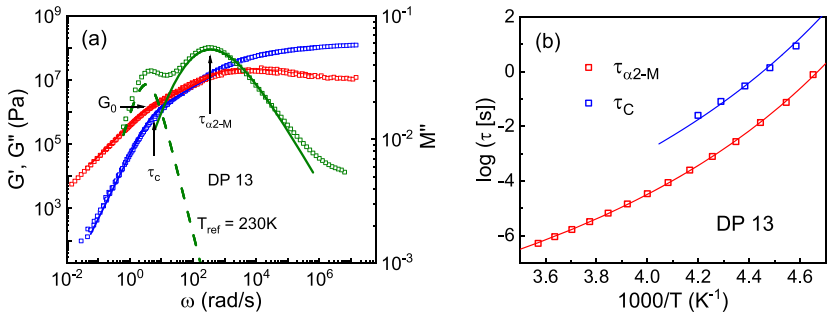

Figure 5. (a) Comparison between the shear modulus (red and blue symbols) and the dielectric loss modulus spectra (green symbols) for PDMS-COOH with DP of 13 sample at 230 K. Terminal relaxation time scale (τ_C) and α_2-relaxation time scale (τ_{α_2-M}) (arrows) are separated by more than one order of magnitude. The low-frequency process (dashed line) in the dielectric modulus spectrum corresponds to conductivity relaxation process with a Debye-like shape. (b) Temperature dependence of the two time scales (symbols) and their fit based on eq 12 and eq 11 (lines).

work,[32] and φ_{int} of DP 19 PDMS-COOH was estimated through

$$\varphi_{int} = \varphi_{cluster}\left[\left(\frac{l_{int}}{R_{cluster}} + 1\right)^3 - 1\right] \quad (9)$$

by using l_{int} = 0.85 nm, the value estimated in our previous studies.[32] The results are in good agreement with the value from mechanical percolation model (~177 MPa), validating that the percolation model explains well the mechanical reinforcement in the studied samples.

Viscoelastic Behavior near Terminal Relaxation. It is interesting that in systems with no percolation (i.e., with DP of 50 and 74), the terminal relaxation demonstrates Maxwellian behavior, that is, the rubbery plateau stops at the terminal relaxation. In contrast, the rubbery plateau in systems with percolating rigid regions (i.e., with DP of 13, 19, and 22) first decreases with a power law before reaching the terminal relaxation (Figure 1a). Consequently, the moduli G_{pl} and G_0 (eq 2) appear to be comparable for nonpercolated systems, while G_{pl} is much higher than G_0 in percolating systems, and the difference increases with decreases in samples DP (Figure 4). Analysis of these data revealed that G_0 obtained from the fit for all the sample follows the classical rubber elasticity[57] predictions for a given length of the PDMS chains (Figure 4), demonstrating that the mechanical reinforcement actually vanishes at terminal relaxation.

To study the viscoelastic properties in phase separated associating polymers, we compared shear modulus spectra and dielectric M″ spectra (Figure 5a). It is evident that τ_c is significantly slower than τ_{α_2-M}, indicating that motion of stickers inside the clusters is not sufficient for terminal relaxation. Interestingly, the shear modulus in percolating systems starts to decrease from the rubbery plateau level at the time scale comparable to τ_{α_2-M} (Figure 5a), suggesting that the stickers motions within the clusters lead to the softening of the modulus down to the level predicted from classical rubber elasticity. Indeed, when chain ends in clusters are unable to move, the whole system is similar to nanoparticles with extremely high grafting density ~1.7−1.9 chains/nm^2 (Table S1). This grafting density is ~3-times higher than in usual polymer grafted nanoparticles, leading to strong crowding and stretching of the chains in the interfacial layer. Stretching of the chain is supported by larger population of the gauche states found from wide-angle X-ray scattering results.[32] All these factors strongly hinder bending of the PDMS segments in the interfacial layer and lead to high modulus. However, when chain ends start to move inside the clusters, the PDMS segments in the interfacial layer can be easily rearranged and change their conformations under external force, and the macroscopic deformation is easier to reach. This results in a gradual softening of the polymer interfacial layer, which is demonstrated through the parallel decrease of the G' and G'' with decrease in frequency. This softening reaches the modulus level expected from the rubber elasticity at the time of the terminal relaxation. Moreover, similar temperature dependences of both τ_{α_2-M} and τ_C (Figures 5b and S7) suggest that dynamics in the clusters might act as a precursor for the macroscopic rearrangement of the network.

Mechanism of Network Rearrangement. The mechanism of network rearrangement in phase separated associating polymers remains a puzzle. It is obvious that the network rearrangement should involve exchange of the stickers between different clusters.[27,58] On the basis of computer simulations, Amin et al. suggested that exchange should go through a merge of different clusters.[27] This mechanism was questioned by Mordvinkin et al.,[28,29] where telechelic poly(isobutylene) (PIB) with functional end groups was studied. These systems, like the polymers studied here, have well-separated clusters, and merging of these clusters is not feasible due to the presence of multiple chains between the clusters. These systems, however, are similar to phase separating triblock copolymers. In phase separating triblock copolymers, network rearrangement process is dominated by a chain pullout process, which needs to overcome the free energy penalty from the immiscibility of different blocks.[58−60] In other words, the block in the phase separated cores needs to be pulled out and diffuse to another phase-separated core to complete the rearrangement process. According to refs 61−63, the pullout time scale is expressed as

$$\tau_{pullout} = \tau_{Rouse}\exp(\alpha\chi N_{core}) \quad (10)$$

in which τ_{Rouse} is Rouse relaxation time of the block inside the phase separated cores. χ is the Flory−Huggins parameter. N_{core} is the number of Kuhn segments of the block forming phase-separated cores. α is a constant in the order of unity. We hypothesize that the similar mechanism controls bond rearrangements in the studied telechelic systems, and the free energy barrier to "chain end pullout" process determines the network rearrangement process.

https://doi.org/10.1021/acsnano.2c00046
ACS Nano XXXX, XXX, XXX−XXX

Borrowing the idea of chain exchange kinetics in block copolymer micelles,[58−60,64] relationship between τ_c and τ_{α_2-M} can be expressed as

$$\tau_c(T) = \tau_{\alpha_2-M}(T)\exp\left(\frac{E_a}{RT}\right) = \tau_{\alpha_2-M}(T)\exp(\alpha\chi N_{core}) \quad (11)$$

in which the activation energy barrier, E_a, is related to the thermodynamic penalty for the sticker to be placed in the polymer matrix $\sim\alpha\chi N_{core}$. To estimate the activation barrier from the experimental result, $\tau_{\alpha_2-M}(T)$ was fit to the Vogel−Fulcher−Tammann (VFT) eq (Figure 5b, red line):

$$\tau_{\alpha_2-M}(T) = \tau_0\exp\left(\frac{B}{T-T_0}\right) \quad (12)$$

Here τ_0, B, and T_0 are the VFT fit parameters. Then $\tau_C(T)$ was fitted using eq 11, in which τ_{α_2-M} was substituted by the VFT equation, with the energy barrier E_a as the only free fit parameter (Figure 5b). The fitting results revealed the average activation energy to be ∼6.6 kJ/mol (Figure 6). Strong deviation in the case of the sample with DP 74 might be caused by crystallization that strongly limited the studied temperature range.

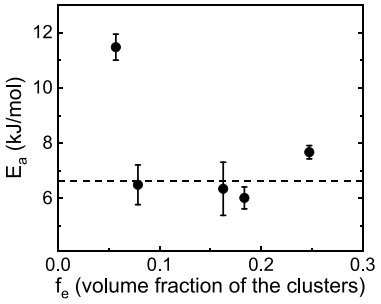

Figure 6. Estimated energy barrier for single sticker "pullout" into PDMS matrix. The solid dashed line indicates the average activation energy for this process. Value for the lowest f_e data is not reliable due to possible sample crystallization.

The obtained activation energy can be compared to the expected $\sim\alpha\chi N_{core}$. N_{core} of the end group is 1, and the Flory−Huggins parameter, χ, can be estimated from the solubility parameters (δ) and molar volume of the chain end instead of the molar volume of a copolymer block:[65]

$$\chi = \frac{(\delta_{end}-\delta_{PDMS})^2 V_{end}}{RT} \quad (13)$$

The solubility parameter of the PDMS backbone δ_{PDMS} is 7.3 $cal^{1/2}$ $cm^{-3/2}$.[66] The solubility parameter of the chain end (COOH), δ_{end}, is estimated to be 11.86 $cal^{1/2}$ $cm^{-3/2}$ via Hansen solubility parameter (HSP)[67] approach, which divides the solubility parameter into three partial components: dispersion, polarity, and hydrogen-bonding (detailed method is mentioned in the Supporting Information). The molar volume of chain ends V_{end} is calculated using $V_{end} = \frac{M_{end}}{\rho_{end}}$, where the molecular weight of chain ends M_{end} is 158 g/mol, and the density of chain ends is assumed to be the same as that of glycerol, ρ_{end} = 1.26 g/cm^3. Thus, $(\delta_{end}-\delta_{PDMS})^2 V_{end}$ is estimated to be ∼11 kJ/mol, in reasonable agreement with the experimentally estimated E_a assuming α value of ∼0.6. The value of α close to 0.6 has been reported in several studies of chain exchange kinetics in different block copolymer micelles.[60,68,69] Thus, the single chain hopping mechanism provides reasonable estimates of the energy barrier controlling terminal relaxation in polymers with phase separated stickers.

On the basis of these results and analysis, we propose the following mechanism of the terminal relaxation in polymers with phase separated reversible bonds (stickers). Network rearrangements require mobility of stickers in the clusters and a sticker escape from the cluster requires to overcome an energy barrier controlled by miscibility of stickers in a polymer matrix. Once the sticker escaped from the cluster, it will diffuse through the polymer matrix to another cluster with a time scale of $\tau_{diffusion}$, which will be mainly governed by Rouse subdiffusive motion, that is, $\tau_{diffusion} \approx \tau_\alpha\left(\frac{d}{l_k}\right)^4$, here d is the distance between clusters (∼5 nm, Tables S1) and l_k is the Kuhn segment length of PDMS (∼1 nm). This provides estimates of $\tau_{diffusion} \approx 10^3\,\tau_\alpha$. At the onset of second T_g, where stickers can move inside the clusters, τ_α is $\sim10^{-9}$ s (Figure S6e) and $\tau_{diffusion}$ is $\sim10^{-6}$ s. This time is many orders faster than terminal relaxation time at the same temperatures. Thus, we can safely assume that sticker escape from the cluster is the rate-determining step in the single chain hopping process. This mechanism is similar to that describing the network rearrangement of Butyl ionomer.[70] However, we introduce the microscopic mechanism of these rearrangements and identify the energy barrier controlling the sticker hopping process. This mechanism also explains the difference between the time scale

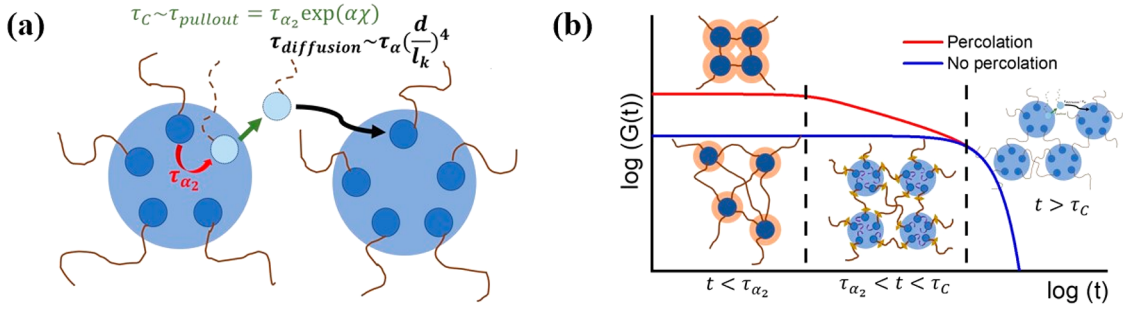

Figure 7. (a) Cartoon of a single chain exchange process between two clusters, which leads to a macroscopic rearrangement of the network. (b) Qualitative picture of the shear modulus variation with time for a phase-separated associated polymer network with percolated interfacial layers (red line) and with no percolation (blue line). Dashed lines mark two important time scales of the system: $\tau_{\alpha 2}$, relaxation in clusters of dynamic bonds; and τ_C, terminal relaxation defined by the network rearrangement time.

https://doi.org/10.1021/acsnano.2c00046
ACS Nano XXXX, XXX, XXX−XXX

of network rearrangement and the dynamic bonds motion inside the clusters. The proposed mechanism is consistent with the recent NMR studies[28,29] revealing that single chain relaxation is responsible for the terminal relaxation in the associating polymer with phase separation. These studies of telechelic PIBs with barbituric acid end groups and with thymine end groups also revealed that cluster relaxation process observed in dielectric spectra is faster than the terminal relaxation, and the ratio of these time scales depends on chemistry of the stickers[29] (Figure S9). Following the proposed mechanism, we estimated the energy barrier (through eq 11) to be $E_a \approx 16-17$ kJ/mol for more polar barbituric acid end groups and ~9 kJ/mol for less polar thymine end group (Table S2). Moreover, these values agree with estimates of $(\delta_{end} - \delta_{PDMS})^2 V_{end}$ (~26 kJ/mol for barbituric acid end group and ~13 kJ/mol for thymine end group) assuming $\alpha \approx 0.6$ (see Supporting Information). Thus, the proposed mechanism also provides good understanding for the network rearrangement in other systems with phase-separated stickers.

General Molecular Picture. On the basis of analysis of the presented above results, we propose a general picture of viscoelasticity in polymers with phase separated dynamic bonds (Figure 7b). Functional end-group clusters possess a higher T_g value than the polymer matrix, and their dynamics is governed by a time scale of structural relaxation in these clusters, τ_{α_2}. At times $t < \tau_{\alpha_2}$, clusters are glassy and control the rubbery plateau level. In such case, not only chain ends are fixed but also the grafting density is extremely high, resulting in chains crowding and stretching in an interfacial layer around these clusters. These severely restrict segmental mobility and chain bending (similar to polymer grafted nanoparticles), leading to a much higher elastic modulus.[32,39] In the absence of percolation of the interfacial polymer regions, the mechanical reinforcement from the interfacial layer is small, and mechanical strength of the associating polymer is mostly defined by the rubber elasticity of network structure cross-linked by the clusters. However, in a case where interfacial regions overlap, significant mechanical reinforcement is observed, which can be ascribed to a percolation phenomenon (Figure 7b). On time scale $\tau_{\alpha_2} < t < \tau_c$, stickers become mobile within the clusters, and even if the grafting density is high, the segments in the vicinity of clusters can easily rearrange and change conformations. This leads to a subsequent decrease of the mechanical modulus in the interfacial layer down to the level expected in the rubber elasticity theory. As a result, the macroscopic modulus level drops down significantly in the case of percolated network as the effect of percolation fades away with the gradual decreasing of the modulus in the interfacial layer. When there is no percolation, the decrease in the shear modulus is negligible until topological reorganization of network occurs at the terminal relaxation time (τ_c). At $t > \tau_c$, sticky ends start to move out of the cluster overcoming the free energy barrier due to their immiscibility with the polymer matrix and subsequently diffuse to another cluster. Through this single chain exchange process, macroscopic stress relaxation happens within the network.

CONCLUSIONS

In this study, we investigated telechelic PDMS with functional groups phase-separating in clusters due to their immiscibility with the polymer backbone. We demonstrated that mechanical percolation model describes well the strong mechanical reinforcement observed in these systems. Although the result is similar to what we achieved earlier using mechanical ILM,[32] the percolation model is more appropriate to explain the mechanical reinforcement since interfacial layers overlap in most of the studied samples. Moreover, our results and analysis question the proposed earlier mechanism[27] of network relaxation through a merger of phase-separated clusters. Instead, we propose a chain-hopping mechanism of network rearrangement borrowed from the field of block copolymer. It provides a reasonably good description of the presented data even on a quantitative level. This mechanism also describes earlier data on telechelic PIB.[29] Finally, we formulate a general molecular picture describing the viscoelastic behavior of associating polymers. When phase separated clusters are frozen, the system behaves as a permanent network, which show strong mechanical reinforcement depending on whether there is percolation. Then the softening of the interfacial layer occurs upon the motion of functional groups inside the phase separated clusters, followed by the network rearrangement controlled by additional energy barrier defined by immiscibility of stickers and polymer matrix.

The presented analysis and the proposed mechanism provide a detailed understanding of the viscoelastic behavior of polymers with phase-separated reversible bonds. These mechanisms should work not only for telechelic associating polymers but also for any associating polymer having phase separating dynamic bonds. The developed understanding is of paramount importance for rational design of advanced materials with enhanced mechanical properties, and better recyclability.

METHODS

Synthesis of PDMS-COOH Polymers. Synthesis of PDMS-COOH polymers was described in detail in our pervious publication.[24,39] The synthesis route is shown in Scheme 1 in Xing et al.[24] DP 19 PDMS-COOH was synthesized in this work. Five grams of PDMS-NH_2 (5 mmol, Gelest Inc. DMS-A11) was added into a flame-dried 100 mL round-bottom flask, and then 2 g of succinic anhydride (20 mmol) was also added followed by the addition of 1.518 g of triethylamine (15 mmol), 0.611 g of 4-dimethylaminopyridine (5 mmol), and 30 mL tetrahydrofuran (THF). The reaction was conducted under an N_2 atmosphere at 40 °C for 2 days. After the reaction was completed, THF was removed by rotary evaporation. Ten milliliters of 1 M hydrochloric acid was added, a total amount of 50 mL of dichloromethane (DCM) was utilized to extract the product from the aqueous solution three times. The organic layer was collected and was removed by rotary evaporation. The final product was obtained and dried in a vacuum oven to remove all residual solvents. ^{1}H NMR was utilized to confirm the final product with $CDCl_3$ as solvent. The chemical structure and the ^{1}H NMR spectra analysis is shown in Figure S2.

Differential Scanning Calorimetry (DSC) Measurements. DSC was employed to probe the glass transition temperature (T_g) of PDMS-COOH using a Q2500 DSC equipment from TA Instruments. The samples were dried in a vacuum oven at 333 K overnight before being placed into DSC pans. The samples were first equilibrated isothermally at 363 K for 10 min to remove the thermal history before being quenched to 113 K (to avoid crystallization). After equilibration for 10 min, the samples were heated up to 293 K with a rate of 10 K/min. This procedure was repeated twice for each sample to ensure repeatability.

X-ray Scattering. X-ray scattering spectra for DP 13, 22, 50, and 74 PDMS-COOH, as well as the reference sample PDMS-CH_3, were measured previously. The procedure was described in detail in ref 32. The DP 19 PDMS-COOH was measured on XEUSS 3.0 (Xenocs,

https://doi.org/10.1021/acsnano.2c00046
ACS Nano XXXX, XXX, XXX−XXX

France) equipped with a Cu Kα microfocus source and a Pilatus 300k detector (Dectris, Switzerland). The scattering vector (q) was calibrated by a silver behenate standard material. The distance between sample and detector was 0.9 m and 0.55 m for SAXS and WAXS, respectively. The sample was squeezed into a capillary tube made of quartz glass with diameter 1.5 mm and wall thickness 0.01 mm. Then the capillary was placed perpendicularly to the X-ray beam. The measurement mentioned above was also done on the empty capillary to subtract the background. X-ray measurements were performed at room temperature.

Broadband Dielectric Spectroscopy (BDS). BDS in the frequency range from 10^{-2} to 10^{6} Hz was measured utilizing a Novocontrol system that includes an Alpha-A impedance analyzer and a Quatro Cryosystem temperature control unit. DP 13, 22, 50, and 74 PDMS-COOH were placed into a parallel-plate dielectric cell made of sapphire and invar steel with an electrode diameter of 12 mm, and capacitance 20 pF with an electrode separation of 50 μm. DP 19 PDMS-COOH was placed into a parallel plate dielectric cell made of sapphire and invar steel with an electrode diameter of 10 mm, and capacitance 3.3 pF with an electrode separation of 210 μm. To prevent crystallization, all samples were quenched from room temperature to about 113 K and reheated to 10 K below the T_g before the measurements. All the spectra were measured on heating. After each temperature increase, the samples were equilibrated for 10 min to reach thermal stabilization within 0.1 K.

Small-Amplitude Oscillatory Shear (SAOS) Measurement. SAOS measurement was utilized to probe the viscoelastic properties of telechelic PDMS-COOH through a strain-controlled mode of the AR2000ex (TA Instruments) with an angular frequency range from 10^{2} to 10^{-1} rad/s using parallel plate geometry with a disk diameter of 4 mm at a variety of temperatures range from second T_g to temperatures that the sample can flow freely. The strain amplitude during the measurement was chosen to be in the range from 0.2% to 5% depending on the modulus level at different temperatures.

ASSOCIATED CONTENT

Supporting Information

The Supporting Information is available free of charge at https://pubs.acs.org/doi/10.1021/acsnano.2c00046.

Chemical structure; DSC results; X-ray scattering spectrum; structural information; rheological shift factors; dielectric spectra; energy barrier estimation; δ_{end} estimation; activation energy estimation (PDF)

AUTHOR INFORMATION

Corresponding Authors

Subarna Samanta − *Department of Chemistry, University of Tennessee, Knoxville, Tennessee 37996, United States;* Email: ssamant2@utk.edu

Alexei P. Sokolov − *Department of Chemistry, University of Tennessee, Knoxville, Tennessee 37996, United States; Chemical Sciences Division, Oak Ridge National Laboratory, Oak Ridge, Tennessee 37830, United States;* orcid.org/0000-0002-8187-9445; Email: sokolov@utk.edu

Authors

Sirui Ge − *Department of Material Science and Engineering, University of Tennessee, Knoxville, Tennessee 37996, United States;* orcid.org/0000-0002-4276-7838

Bingrui Li − *The Bredesen Center for Interdisciplinary Research and Graduate Education, University of Tennessee, Knoxville, Tennessee 37996, United States;* orcid.org/0000-0002-4974-5826

G. Peyton Carden − *Department of Chemistry, University of Tennessee, Knoxville, Tennessee 37996, United States*

Peng-Fei Cao − *Chemical Sciences Division, Oak Ridge National Laboratory, Oak Ridge, Tennessee 37830, United States;* orcid.org/0000-0003-2391-1838

Complete contact information is available at: https://pubs.acs.org/10.1021/acsnano.2c00046

Notes

The authors declare no competing financial interest.

ACKNOWLEDGMENTS

We thank the NSF Polymer program for the financial support of these studies (BDS, rheology, DSC, and data analysis) under Award No. DMR-1904657. B.L. and P.-F.C. acknowledge support for synthesis by the DOE BES Materials Science and Technology Division. X-ray measurements were enabled by the Major Research Instrumentation program of the National Science Foundation under Award No. DMR-1827474.

REFERENCES

(1) Bowman, C. N.; Kloxin, C. J. Covalent adaptable networks: reversible bond structures incorporated in polymer networks. *Angew. Chem., Int. Ed.* **2012**, *51* (18), 4272−4274.

(2) Chakma, P.; Konkolewicz, D. Dynamic covalent bonds in polymeric materials. *Angew. Chem.* **2019**, *131* (29), 9784−9797.

(3) Zheng, N.; Xu, Y.; Zhao, Q.; Xie, T. Dynamic Covalent Polymer Networks: A Molecular Platform for Designing Functions beyond Chemical Recycling and Self-Healing. *Chem. Rev.* **2021**, *121* (3), 1716−1745.

(4) Nakahata, M.; Takashima, Y.; Yamaguchi, H.; Harada, A. Redox-responsive self-healing materials formed from host-guest polymers. *Nat. Commun.* **2011**, *2* (1), 1−6.

(5) Sun, T. L.; Kurokawa, T.; Kuroda, S.; Ihsan, A. B.; Akasaki, T.; Sato, K.; Haque, M. A.; Nakajima, T.; Gong, J. P. Physical hydrogels composed of polyampholytes demonstrate high toughness and viscoelasticity. *Nature materials* **2013**, *12* (10), 932−937.

(6) Chen, Y.; Kushner, A. M.; Williams, G. A.; Guan, Z. Multiphase design of autonomic self-healing thermoplastic elastomers. *Nature Chem.* **2012**, *4* (6), 467−472.

(7) Whittell, G. R.; Hager, M. D.; Schubert, U. S.; Manners, I. Functional soft materials from metallopolymers and metallosupramolecular polymers. *Nature materials* **2011**, *10* (3), 176−188.

(8) Burattini, S.; Greenland, B. W.; Merino, D. H.; Weng, W.; Seppala, J.; Colquhoun, H. M.; Hayes, W.; Mackay, M. E.; Hamley, I. W.; Rowan, S. J. A healable supramolecular polymer blend based on aromatic π- π stacking and hydrogen-bonding interactions. *J. Am. Chem. Soc.* **2010**, *132* (34), 12051−12058.

(9) Li, C.-H.; Wang, C.; Keplinger, C.; Zuo, J.-L.; Jin, L.; Sun, Y.; Zheng, P.; Cao, Y.; Lissel, F.; Linder, C.; et al. A highly stretchable autonomous self-healing elastomer. *Nature Chem.* **2016**, *8* (6), 618−624.

(10) Cao, P. F.; Li, B.; Hong, T.; Townsend, J.; Qiang, Z.; Xing, K.; Vogiatzis, K. D.; Wang, Y.; Mays, J. W.; Sokolov, A. P.; et al. Superstretchable, Self-Healing Polymeric Elastomers with Tunable Properties. *Adv. Funct. Mater.* **2018**, *28* (22), 1800741.

(11) Peng, W.; Zhang, G.; Zhao, Q.; Xie, T. Autonomous Off-Equilibrium Morphing Pathways of a Supramolecular Shape-Memory Polymer. *Adv. Mater.* **2021**, *33*, 2102473.

(12) Cooper, C. B.; Nikzad, S.; Yan, H.; Ochiai, Y.; Lai, J.-C.; Yu, Z.; Chen, G.; Kang, J.; Bao, Z. High Energy Density Shape Memory Polymers Using Strain-Induced Supramolecular Nanostructures. *ACS Central Science* **2021**, *7*, 1657.

(13) Qin, B.; Zhang, S.; Sun, P.; Tang, B.; Yin, Z.; Cao, X.; Chen, Q.; Xu, J. F.; Zhang, X. Tough and multi-recyclable cross-linked supramolecular polyureas via incorporating noncovalent bonds into main-chains. *Adv. Mater.* **2020**, *32* (36), 2000096.

(14) Cordier, P.; Tournilhac, F.; Soulié-Ziakovic, C.; Leibler, L. Self-healing and thermoreversible rubber from supramolecular assembly. *Nature* **2008**, *451* (7181), 977−980.
(15) Ge, S.; Tress, M.; Xing, K.; Cao, P.-F.; Saito, T.; Sokolov, A. P. Viscoelasticity in associating oligomers and polymers: experimental test of the bond lifetime renormalization model. *Soft Matter* **2020**, *16* (2), 390−401.
(16) Keten, S.; Xu, Z.; Ihle, B.; Buehler, M. J. Nanoconfinement controls stiffness, strength and mechanical toughness of β-sheet crystals in silk. *Nature materials* **2010**, *9* (4), 359−367.
(17) Du, N.; Yang, Z.; Liu, X. Y.; Li, Y.; Xu, H. Y. Structural origin of the strain-hardening of spider silk. *Adv. Funct. Mater.* **2011**, *21* (4), 772−778.
(18) Deng, Y.; Zhang, Q.; Feringa, B. L.; Tian, H.; Qu, D. H. Toughening a self-healable supramolecular polymer by ionic cluster-enhanced iron-carboxylate complexes. *Angew. Chem.* **2020**, *132* (13), 5316−5321.
(19) Lai, Y.; Kuang, X.; Zhu, P.; Huang, M.; Dong, X.; Wang, D. Colorless, transparent, robust, and fast scratch-self-healing elastomers via a phase-locked dynamic bonds design. *Adv. Mater.* **2018**, *30* (38), 1802556.
(20) Wan, D.; Jiang, Q.; Song, Y.; Pan, J.; Qi, T.; Li, G. L. Biomimetic Tough Self-Healing Polymers Enhanced by Crystallization Nanostructures. *ACS Applied Polymer Materials* **2020**, *2* (2), 879−886.
(21) Middleton, L. R.; Winey, K. I. Nanoscale aggregation in acid- and ion-containing polymers. *Annu. Rev. Chem. Biomol. Eng.* **2017**, *8*, 499−523.
(22) Goldansaz, H.; Fustin, C.-A.; Wübbenhorst, M.; Van Ruymbeke, E. How supramolecular assemblies control dynamics of associative polymers: Toward a general picture. *Macromolecules* **2016**, *49* (5), 1890−1902.
(23) Yan, T.; Schröter, K.; Herbst, F.; Binder, W. H.; Thurn-Albrecht, T. Unveiling the molecular mechanism of self-healing in a telechelic, supramolecular polymer network. *Sci. Rep.* **2016**, *6* (1), 1−8.
(24) Xing, K.; Tress, M.; Cao, P.; Cheng, S.; Saito, T.; Novikov, V. N.; Sokolov, A. P. Hydrogen-bond strength changes network dynamics in associating telechelic PDMS. *Soft Matter* **2018**, *14* (7), 1235−1246.
(25) Liu, Y.; Tang, Z.; Wang, D.; Wu, S.; Guo, B. Biomimetic design of elastomeric vitrimers with unparalleled mechanical properties, improved creep resistance and retained malleability by metal-ligand coordination. *Journal of Materials Chemistry A* **2019**, *7* (47), 26867−26876.
(26) Tress, M.; Xing, K.; Ge, S.; Cao, P.; Saito, T.; Sokolov, A. What dielectric spectroscopy can tell us about supramolecular networks. *Eur. Phys. J. E* **2019**, *42* (10), 133.
(27) Amin, D.; Likhtman, A. E.; Wang, Z. Dynamics in Supramolecular Polymer Networks Formed by Associating Telechelic Chains. *Macromolecules* **2016**, *49* (19), 7510−7524.
(28) Mordvinkin, A.; Döhler, D.; Binder, W. H.; Colby, R. H.; Saalwächter, K. Terminal Flow of Cluster-Forming Supramolecular Polymer Networks: Single-Chain Relaxation or Micelle Reorganization? *Physical review letters.* **2020**, *125* (12), 127801.
(29) Mordvinkin, A.; Döhler, D.; Binder, W. H.; Colby, R. H.; Saalwächter, K. Rheology, Sticky Chain, and Sticker Dynamics of Supramolecular Elastomers Based on Cluster-Forming Telechelic Linear and Star Polymers. *Macromolecules* **2021**, *54*, 5065.
(30) Vanhoorne, P.; Jérôme, R.; Teyssié, P.; Laupretre, F. Direct NMR evidence for a local restriction in the segmental chain mobility of a model ionomer. *Macromolecules* **1994**, *27* (9), 2548−2552.
(31) Sinha, K.; Maranas, J. K. Segmental dynamics and ion association in PEO-based single ion conductors. *Macromolecules* **2011**, *44* (13), 5381−5391.
(32) Ge, S.; Samanta, S.; Tress, M.; Li, B.; Xing, K.; Dieudonné-George, P.; Genix, A.-C.; Cao, P.-F.; Dadmun, M.; Sokolov, A. P. Critical Role of the Interfacial Layer in Associating Polymers with Microphase Separation. *Macromolecules* **2021**, *54* (9), 4246−4256.
(33) Essam, J. W. Percolation theory. *Rep. Prog. Phys.* **1980**, *43* (7), 833.
(34) Stauffer, D.; Aharony, A. *Introduction to percolation theory*; CRC Press, 2018.
(35) Maurer, F. An interlayer model to describe the physical properties of particulate composites. In *Controlled interphases in composite materials*; Springer, 1990; pp 491−504.
(36) Musino, D.; Genix, A.-C.; Chauveau, E.; Bizien, T.; Oberdisse, J. Structural identification of percolation of nanoparticles. *Nanoscale* **2020**, *12* (6), 3907−3915.
(37) Baeza, G. P.; Dessi, C.; Costanzo, S.; Zhao, D.; Gong, S.; Alegria, A.; Colby, R. H.; Rubinstein, M.; Vlassopoulos, D.; Kumar, S. K. Network dynamics in nanofilled polymers. *Nat. Commun.* **2016**, *7*, 11368.
(38) Nadiv, R.; Fernandes, R. M. F.; Ochbaum, G.; Dai, J.; Buzaglo, M.; Varenik, M.; Biton, R.; Furó, I.; Regev, O. Polymer nanocomposites: Insights on rheology, percolation and molecular mobility. *Polymer* **2018**, *153*, 52−60.
(39) Tress, M.; Ge, S.; Xing, K.; Cao, P.-F.; Saito, T.; Genix, A.-C.; Sokolov, A. P. Turning Rubber into a Glass: Mechanical Reinforcement by Microphase Separation. *ACS Macro Lett.* **2021**, *10*, 197−202.
(40) Ferry, J. D. *Viscoelastic properties of polymers*; John Wiley & Sons, 1980.
(41) Kremer, F.; Schönhals, A. *Broadband dielectric spectroscopy*; Springer Science & Business Media, 2002.
(42) Tarnacka, M.; Jurkiewicz, K.; Hachuła, B.; Wojnarowska, Z.; Wrzalik, R.; Bielas, R.; Talik, A.; Maksym, P.; Kaminski, K.; Paluch, M. Correlation between Locally Ordered (Hydrogen-Bonded) Nanodomains and Puzzling Dynamics of Polymethysiloxane Derivative. *Macromolecules* **2020**, *53* (22), 10225−10233.
(43) Richert, R.; Agapov, A.; Sokolov, A. P. Appearance of a Debye process at the conductivity relaxation frequency of a viscous liquid. *J. Chem. Phys.* **2011**, *134* (10), 104508.
(44) Gainaru, C.; Stacy, E. W.; Bocharova, V.; Gobet, M.; Holt, A. P.; Saito, T.; Greenbaum, S.; Sokolov, A. P. Mechanism of conductivity relaxation in liquid and polymeric electrolytes: Direct link between conductivity and diffusivity. *J. Phys. Chem. B* **2016**, *120* (42), 11074−11083.
(45) Richert, R.; Wagner, H. The dielectric modulus: relaxation versus retardation. *Solid State Ionics* **1998**, *105* (1−4), 167−173.
(46) Kremer, F.; Schönhals, A. *Broadband Dielectric Spectroscopy*; Springer-Verlag; Berlin, 2003.
(47) Favier, V.; Cavaille, J.; Canova, G.; Shrivastava, S. Mechanical percolation in cellulose whisker nanocomposites. *Polym. Eng. Sci.* **1997**, *37* (10), 1732−1739.
(48) De Gennes, P.-G. On a relation between percolation theory and the elasticity of gels. *J. Phys., Lett.* **1976**, *37* (1), 1−2.
(49) Tokita, M.; Niki, R.; Hikichi, K. Percolation theory and elastic modulus of gel. *J. Phys. Soc. Jpn.* **1984**, *53* (2), 480−482.
(50) Evingür, G. A.; Pekcan, Ö. Elastic percolation of swollen polyacrylamide (PAAm)-multiwall carbon nanotubes composite. *Phase Transitions* **2012**, *85* (6), 553−564.
(51) Djabourov, M.; Leblond, J.; Papon, P. Gelation of aqueous gelatin solutions. II. Rheology of the sol-gel transition. *J. Phys. (Paris)* **1988**, *49* (2), 333−343.
(52) Hsu, W. Y.; Wu, S. Percolation behavior in morphology and modulus of polymer blends. *Polym. Eng. Sci.* **1993**, *33* (5), 293−302.
(53) Gauthier-Manuel, B.; Guyon, E. Critical, elasticity of polyacrylamide above its gel point. *J. Phys., Lett.* **1980**, *41* (21), 503−505.
(54) Le Strat, D.; Dalmas, F.; Randriamahefa, S.; Jestin, J.; Wintgens, V. Mechanical reinforcement in model elastomer nanocomposites with tuned microstructure and interactions. *Polymer* **2013**, *54* (5), 1466−1479.
(55) Müller, A.; Wapler, M. C.; Wallrabe, U. A quick and accurate method to determine the Poisson's ratio and the coefficient of thermal expansion of PDMS. *Soft Matter* **2019**, *15* (4), 779−784.
(56) Lyapin, A. G.; Gromnitskaya, E. L.; Danilov, I. V.; Brazhkin, V. V. Elastic properties of the hydrogen-bonded liquid and glassy

https://doi.org/10.1021/acsnano.2c00046
ACS Nano XXXX, XXX, XXX−XXX

glycerol under high pressure: comparison with propylene carbonate. *RSC Adv.* **2017**, *7* (53), 33278−33284.
(57) Hayashi, M.; Noro, A.; Matsushita, Y. Viscoelastic properties of supramolecular soft materials with transient polymer network. *J. Polym. Sci., Part B: Polym. Phys.* **2014**, *52* (11), 755−764.
(58) Ma, Y.; Lodge, T. P. Chain exchange kinetics in diblock copolymer micelles in ionic liquids: The role of χ. *Macromolecules* **2016**, *49* (24), 9542−9552.
(59) Wang, E.; Lu, J.; Bates, F. S.; Lodge, T. P. Effect of corona block length on the structure and chain exchange kinetics of block copolymer micelles. *Macromolecules* **2018**, *51* (10), 3563−3571.
(60) Wang, E.; Zhu, J.; Zhao, D.; Xie, S.; Bates, F. S.; Lodge, T. P. Effect of solvent selectivity on chain exchange kinetics in block copolymer micelles. *Macromolecules* **2020**, *53* (1), 417−426.
(61) Lu, J.; Bates, F. S.; Lodge, T. P. Remarkable effect of molecular architecture on chain exchange in triblock copolymer micelles. *Macromolecules* **2015**, *48* (8), 2667−2676.
(62) Peters, A. J.; Lodge, T. P. Comparison of gel relaxation times and end-block pullout times in ABA triblock copolymer networks. *Macromolecules* **2016**, *49* (19), 7340−7349.
(63) Zhao, D.; Ma, Y.; Lodge, T. P. Exchange kinetics for a single block copolymer in micelles of two different sizes. *Macromolecules* **2018**, *51* (6), 2312−2320.
(64) Lu, J.; Bates, F.; Lodge, T. Chain exchange in binary copolymer micelles at equilibrium: confirmation of the independent chain hypothesis. *ACS Macro Lett.* **2013**, *2* (5), 451−455.
(65) Chremos, A.; Nikoubashman, A.; Panagiotopoulos, A. Z. Flory-Huggins parameter χ, from binary mixtures of Lennard-Jones particles to block copolymer melts. *J. Chem. Phys.* **2014**, *140* (5), 054909.
(66) Lee, J. N.; Park, C.; Whitesides, G. M. Solvent Compatibility of Poly(dimethylsiloxane)-Based Microfluidic Devices. *Anal. Chem.* **2003**, *75* (23), 6544−6554.
(67) Hansen, C. M. *Hansen solubility parameters: a user's handbook*; CRC Press, 2007.
(68) Choi, S.-H.; Lodge, T. P.; Bates, F. S. Mechanism of molecular exchange in diblock copolymer micelles: hypersensitivity to core chain length. *Physical review letters* **2010**, *104* (4), 047802.
(69) Kim, S.; Lee, S.; Choi, S.-H.; Char, K. Chain Exchange Kinetics of Bottlebrush Block Copolymer Micelles. *Macromolecules* **2021**, *54* (10), 4739−4746.
(70) Mordvinkin, A.; Suckow, M.; Böhme, F.; Colby, R. H.; Creton, C.; Saalwächter, K. Hierarchical Sticker and Sticky Chain Dynamics in Self-Healing Butyl Rubber Ionomers. *Macromolecules* **2019**, *52* (11), 4169−4184.

https://doi.org/10.1021/acsnano.2c00046
ACS Nano XXXX, XXX, XXX−XXX